Examining single-source secondary impacts estimated from brute-force, decoupled direct method, and advanced plume treatment approaches

James T. Kelly[1], Kirk R. Baker[1], Sergey L. Napelenok[2], and Shawn J. Roselle[2]

[1]*Office of Air Quality Planning and Standards, U.S. EPA, Research Triangle Park, NC, USA*

[2]*Office of Research and Development, U. S. EPA, Research Triangle Park, NC, USA*

Correspondence to
James T Kelly
Air Quality Modeling Group | Air Quality Assessment Division
Office of Air Quality Planning & Standards | Office of Air & Radiation
US Environmental Protection Agency
109 TW Alexander Drive | Mail Drop: C439-01
Research Triangle Park, NC 27711
Tel: (919) 541-0886 | Fax: (919) 541-0044 | Email: kelly.james@epa.gov

Abstract

In regulatory assessments, there is a need for reliable estimates of the impacts of precursor emissions from individual sources on secondary $PM_{2.5}$ (particulate matter with aerodynamic diameter less than 2.5 microns) and ozone. Three potential methods for estimating these impacts using Eulerian grid photochemical models are the brute-force (B-F) method, the decoupled direct method (DDM), and advanced plume treatment (APT). Here, we systematically inter-compare and assess the B-F, DDM, and APT approaches using hypothetical sources in a consistent modeling platform for a wide range of source conditions (i.e., emissions amount and composition, location, and stack parameters). The impacts of NOx and VOC sources on ozone and SO_2 sources on $PM_{2.5}$ sulfate calculated by these methods are in general agreement. The agreement is evident in the similar magnitudes, spatial patterns, and strong correlations among the impacts. This result, along with previous model evaluations based on similar Eulerian grid modeling, builds confidence in the reliability of the impact estimates. Disagreement among methods is evident in calculations of $PM_{2.5}$ nitrate impacts associated with NH_3 and NOx sources. Numerical instabilities in DDM sensitivity calculations compromise the nitrate impact estimates from that approach. The B-F and APT methods, which use brute-force differencing to identify impacts, are affected by numerical artifacts to a lesser degree than (H)DDM, with the artifacts being more prominent for APT than B-F. Overall, our results indicate that the (H)DDM, B-F, and APT approaches are viable for use in estimating single-source impacts for ozone and secondary $PM_{2.5}$ sulfate, while the B-F method appears to be the most reliable for estimating nitrate impacts. There is a need for additional field study measurements to better constrain model estimates of single-source secondary impacts.

Keywords: single source impacts, plume in grid, decoupled direct method, California, $PM_{2.5}$

1. Introduction

Estimates of the impacts of emissions from individual sources on ozone and secondary particulate matter (PM formed *in situ*) are useful in a variety of contexts. In permit modeling applications related to the National Environmental Policy Act and the Clean Air Act's New Source Review and Prevention of Significant Deterioration provisions, estimates of source contributions to secondary pollutants are needed (e.g., U. S. EPA, 2012a, 2014). Information on single-source secondary impacts (SSIs) could also be useful for informing air quality management approaches involving emissions trading among different sources and/or pollutants. Although State Implementation Plans (SIPs) for achieving national ambient air quality standards (NAAQS) are commonly based on emission reductions from a collection of sources, the design of an emission control plan targeting secondary pollutants can be guided by an understanding of the impacts of individual sources. Similarly, the development of control strategies for the Regulatory Impact Analyses associated with NAAQS revisions could be informed by knowledge of SSIs. However, this knowledge is limited due to challenges in modeling the wide range of relevant length scales and chemical processes, and the impacts of single sources on air quality are commonly estimated in permit applications using models that do not account for important nonlinear atmospheric chemistry (e.g., AERMOD; Cimorelli et al., 2004).

The most straightforward way to estimate SSIs may be the brute-force (B-F) method using an Eulerian grid photochemical model such as the Community Multiscale Air Quality (CMAQ; Byun and Schere, 2006) model or the Comprehensive Air Quality Model with Extensions (CAMx; Environ, 2014). These models include state-of-the-science representations of secondary pollutant formation within a three-dimensional fixed grid domain. In the B-F method, the impacts of a source are estimated by subtracting the results of a simulation where the source's emissions are removed (i.e., "zeroed-out") from one where the emissions are included. Advantages of this approach are that the models are robust and routinely applied in regulatory applications for secondary pollutants, the chemistry simulation occurs at the same spatial scale as the model inputs for meteorology and terrain, and the background atmosphere is chemically realistic. However, the instantaneous dilution of point source emissions into a grid

cell in this method can cause mischaracterization of the transport and chemistry of single-source emissions (e.g., Seigneur et al., 1983; Mathur et al., 1992; Gillani and Pleim, 1996; Karamchandani et al., 2002; Korsakissok and Mallet, 2010). In a discussion based on models with 20-80 km horizontal resolution, Gillani and Pleim (1996) indicated that grid-cell dilution can artificially shift the initial plume chemistry from the typical NOx-saturated conditions toward the NOx-limited conditions of the background atmosphere and prohibit simulation of the multiple stages of plume chemistry. These stages are defined by Karamchandani et al. (1998) as (1) O_3 titration by NO to NO_2, (2) secondary acid production, and (3) ozone production under oxidant rich conditions. Gillani and Pleim (1996) and others (e.g., Bergin et al., 2008) have called for finer resolution (~1-4 km) simulations to reduce the influence of grid cell dilution on SSI assessments. Cohan et al. (2006) found that the initial stage of plume chemistry (O_3 titration) was captured in simulations with 4-km horizontal resolution, and Zhou et al. (2012) and Baker and Kelly (2014) found similar behavior in agreement with aircraft observations along downwind transects. Henderson et al. (2010, 2011) reported that an Eulerian grid model with 1-km resolution could represent the impacts of large hypothetical releases of highly reactive volatile organic compounds. Another potential limitation of the B-F approach is that the numerical errors in the two simulations could be inconsistent (uncorrelated) and not cancel sufficiently when the modeled fields are differenced. Therefore results from the B-F method could be influenced by numerical artifacts when applied to estimate impacts for small emission perturbations (Hakami et al, 2004).

The decoupled direct method (DDM) implemented within an Eulerian grid model (i.e., DDM-3D; Yang et al., 1997) can also be used to estimate SSIs. In DDM-3D, the model directly solves the governing equations for the derivatives that are the infinitesimal pollutant responses to a perturbation. When defined as the sensitivity of pollutant concentration to the emissions from a single source, these derivatives can serve as the coefficients in a Taylor polynomial that can be used to estimate the zero-out impact of the source (Cohan et al., 2005). This approach incurs the same grid-cell dilution artifacts as B-F as well as those due to extrapolation of the Taylor polynomial between the source emission level and the zero-out level. However, unlike B-F, it does not suffer from errors associated with subtracting the results of two simulations

that differ only by a potentially small input perturbation. Therefore, DDM-3D based SSIs may be used to benchmark B-F based SSIs in cases of small emissions perturbations, whereas the reverse may be suitable for large emissions perturbations. Also, DDM-3D can be configured to estimate SSIs for many sources in a single simulation, which could be beneficial for efficiently developing comprehensive response surface models. Yet, despite its advantages, the DDM-3D approach is relatively less tested than B-F, especially for secondary PM, and sensitivity calculations can produce numerical errors under some conditions due to difficulties replicating certain cloud and chemistry processes (e.g., Hakami et al., 2004; Cohan et al., 2005).

To reduce errors associated with the dilution of point source emissions in large grid cells, sub-grid plume modeling approaches were developed in the early 1980's (e.g., Seigneur et al., 1983). In modern sub-grid plume treatments, a Lagrangian puff model with full gas and aerosol chemistry is embedded in an Eulerian grid model (e.g., Karamchandani et al., 2011; Environ, 2014). Such advanced plume treatments (APTs) are attractive because they attempt to treat the chemical and physical evolution of point source emissions from the tens-of-meters scale to the Eulerian grid scale (often tens of kilometers). However, since emitted puffs ultimately disappear when their contents are passed to the Eulerian grid model, the B-F method (with associated differencing errors) must be applied to identify the source's impacts in the APT approach. Another limitation of this method is that meteorological and other information at the grid scale are used to transport and disperse puffs that exist at much finer scales (Karamchandani et al., 2011). Artifacts associated with the sudden dumping of puff contents to the grid cell may also occur and have led to "puff leakage" treatments (Environ, 2014). A thorough evaluation of the errors associated with APT and the other approaches is generally not possible due to the lack of comprehensive datasets for characterizing the evolution of single-source emissions. Model performance statistics at routine network monitors typically show similar performance for APT and standard Eulerian grid modeling, particularly for secondary pollutants such as ozone (e.g., Karamchandani et al., 2002, 2014; Korsakissok and Mallet, 2010; Kim et al., 2014). However, improvements in predictions of primary pollutants (i.e., SO_2 and NO) have been found when including APT in Eulerian grid models in some (Karamchandani et al., 2006; Korsakissok and Mallet, 2010) but not all (Baker et al., 2014) cases.

The behavior of the methods described above is difficult to fully characterize from studies in the current literature because (1) they are based on different modeling systems and simulation periods (i.e., comparison across studies is not straightforward); (2) they often assess the combined impacts of multiple sources (i.e., SSIs are not always identified); (3) sources of interest tend to have large emissions (i.e., B-F limitations are not fully tested); and (4) the composition of emissions is based on a few real-world cases (i.e., systematic examination of different hypothetical emission scenarios is not done). Here, we systematically inter-compare and assess the B-F, DDM-3D, and APT approaches for estimating SSIs by simulating the impacts of hypothetical single sources on secondary $PM_{2.5}$ (PM with aerodynamic diameter less than 2.5 μm) and ozone with a consistent modeling platform for a wide range of conditions (i.e., emissions amount and composition, source location, and stack parameters).

2. Methods

CMAQ simulations were conducted using 4-km horizontal resolution and 25 vertical layers on two domains in California (Fig. 1) for winter and summer time periods (~10 days each; Table 1) in 2007. The modeling domains, one over the South Coast Air Basin (SoCAB) and one over the San Joaquin Valley (SJV), were selected because (1) these areas are conducive to ozone and PM formation; (2) they include a wide range of challenging meteorology, chemistry, and terrain conditions; (3) they contain inorganic PM impacted by all major ions; and (4) they enable us to leverage understanding of air pollution processes developed previously for these regions (e.g., Pusede and Cohen, 2012; Baker et al., 2013; Ryerson et al., 2013; Kelly et al., 2014).

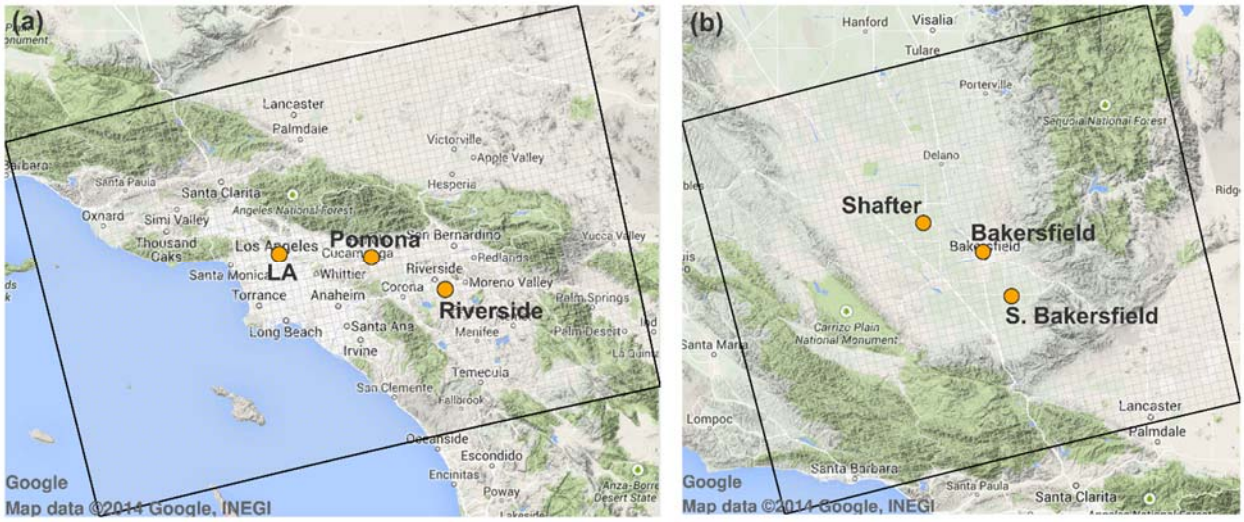

Fig. 1. Modeling domains and hypothetical source locations: (a) SoCAB and (b) San Joaquin Valley.

Table 1. Summary of single-source modeling scenarios.

Parameter	Description
Models[a,b]	CMAQ, CMAQ-(H)DDM, and CMAQ-APT
Domains	SoCAB and SJV
Periods	SoCAB: 1-10 July and 2-12 November 2007 SJV: 1-10 July and 17-27 January 2007
Sources	SoCAB: LA, Pomona, and Riverside SJV: Shafter, Bakersfield, and S. Bakersfield
Emission cases[c,d,e]	NOx, VOC, NH_3, Primary $PM_{2.5}$, and SO_2
Emission amounts[f]	100 and 500 t yr^{-1}
Release heights[g]	Near-surface and aloft

[a]Version 5.0.2

[b]First- and second-order sensitivities were used with CMAQ-HDDM for NOx releases; first-order sensitivities were used for other cases.

[c]Primary $PM_{2.5}$ emissions were represented by elemental carbon; NOx emissions were 15% NO_2 and 85% NO by mass; see Table S1 for the VOC profile based on the average profile in the SPECIATE database (http://www.epa.gov/ttnchie1/software/speciate/).

[d]VOC emissions cases were not simulated with CMAQ-(H)DDM for the November and January scenarios.

[e]For the November simulation with the Riverside source, primary $PM_{2.5}$ and SO_2 emissions cases were not simulated with CMAQ-APT and the aloft NH_3 source (100 t yr^{-1}) simulation was incomplete.

[f]Emissions are reported in short tons

[g]See Table 2 for stack parameters

166 Table 2. Stack parameters for near-surface and aloft releases[a].

Parameter	Near-surface	Aloft
Height (m)	1	75
Diameter (m)	3	3
Temperature (K)	293	420
Exit velocity (m/s)	0.1	20

167 [a]See Figs. S1 and S2 for average vertical emission profiles
168

169 Three versions of CMAQ were applied in this study: standard CMAQv5.0.2, CMAQv5.0.2
170 with DDM-3D (Napelenok et al., 2008; Zhang et al., 2012), and a pre-release version of
171 CMAQv5.0.2 with advanced plume treatment (CMAQ-APT; Karamchandani et al., 2014). In all
172 cases, gas-phase chemistry was simulated using the CB05 mechanism with toluene and chlorine
173 updates (Whitten et al., 2010; Yarwood et al., 2005), and aerosol chemistry was treated with
174 the AERO6 module. Anthropogenic emissions were based on the 2008 National Emissions
175 Inventory, version 2, and biogenic emissions were based on the Biogenic Emissions Inventory
176 System, version 3.14. Meteorological fields used to drive the CMAQ simulations were
177 generated with the Weather Research and Forecasting (WRF) model, version 3.3 (Skamarock et
178 al., 2008). Initial and boundary chemical fields for the CMAQ simulations were derived from an
179 annual 4-km simulation on a statewide domain that was nested within a continental scale 12-
180 km domain. Additional details on the CMAQ and WRF configurations and the emissions
181 inventory are available elsewhere (U.S. EPA, 2012b, 2013a, 2013b).

182 The B-F based impacts were calculated as described above by subtracting the results of
183 a simulation with the source's emissions removed from one including the source. Conceptually,
184 this approach replicates the change in air quality associated with a new source being
185 introduced into a region. The DDM-3D based impacts were calculated from the semi-
186 normalized sensitivities to full source emissions. First-order sensitivities were used for all cases
187 except for the NOx emissions cases, where higher-order sensitivities (i.e., second order; HDDM-
188 3D) were also used. Second-order sensitivities were used for the NOx emissions cases due to
189 the greater nonlinearity of ozone response to these emissions than VOC and other emissions
190 (e.g., Hakami et al., 2003, 2004). SSIs were estimated from the (H)DDM-3D results by

191 extrapolating the pollutant sensitivities from the full emissions level to the zero-out level as
192 described by Cohan et al. (2005).

193 CMAQ-APT was applied using its default configuration where material in the Lagrangian
194 puffs is transferred to the Eulerian grid when the horizontal dimensions of the puff are
195 commensurate with the horizontal resolution of the grid cell (Karamchandani et al., 2014). To
196 estimate single-source impacts using the CMAQ-APT model output, material from active (non-
197 transferred) puffs was first combined with the Eulerian grid concentrations using the post-
198 processor described by Karamchandani et al. (2014). Results from a reference CMAQ-APT
199 simulation with reactive emissions from the source removed were then subtracted from these
200 merged fields.

201 The periods 1-10 July and 2-12 November 2007 were selected for sources in the SoCAB
202 domain due to the conducive conditions for ozone (July) and secondary $PM_{2.5}$ (November)
203 formation. Similarly, the 1-10 July and 17-27 January 2007 periods were selected for simulating
204 hypothetical sources in the SJV domain. Observed levels of ozone and $PM_{2.5}$ at monitors in
205 SoCAB and SJV during these periods are provided in section 2 of the Supplementary Material.
206 Three sources were introduced into each domain (Fig. 1) in separate simulations to estimate
207 the impacts of emissions under different atmospheric conditions. For the SoCAB domain,
208 sources were added in LA (latitude: 34.065°, longitude: -118.228°), Pomona (34.051°, -
209 117.732°), and Riverside (33.904°, -117.335°) to capture the gradient in conditions (e.g., VOC-
210 to-NOx ratio) from the urban core (LA) to a downwind receptor (Riverside). For the SJV domain,
211 sources were added in Shafter (35.514°, -119.338°), Bakersfield (35.391°, -119.026°), and south
212 of Bakersfield (35.198°, -118.877°). These locations span a range of atmospheric conditions
213 from upwind (Shafter) to downwind (S. Bakersfield) of Bakersfield.

214 Five pure emission scenarios (i.e., NOx, VOC, NH_3, primary PM, and SO_2) were simulated
215 with the B-F, (H)DDM, and APT approaches, and three binary mixture scenarios (i.e., NOx+VOC,
216 NOx+NH_3, and NH_3+VOC) were simulated with the B-F method. SSIs for the mixture scenarios
217 generally agreed with the linear combinations of SSIs from the corresponding pure emissions
218 scenarios and are not discussed further. While the full suite of simulations was completed with

the standard B-F approach, several cases (see Table 1 footnotes) were not simulated with (H)DDM and APT due to computational limitations and the likelihood that these simulations would provide limited additional insights. Emission levels of 100 and 500 t yr^{-1} were simulated for each scenario. These emission levels are smaller than those used in most previous studies and test the ability of brute-force differencing methods to identify the plume signal. For each scenario, simulations were conducted with stacks designed for near-surface and aloft releases (Table 2). Due to the large number of simulations, a comprehensive discussion of all results is not possible. Therefore we focus on the most important study findings below, and additional results are provided in the Supplementary Material.

3. **Results and Discussion**

Model performance was evaluated for the reference case simulations (i.e., no hypothetical source emissions) using available observations (see Supplementary Material, Section 2). In general, ozone concentrations predicted by the model agree well with observations during the 1-10 July period in both SoCAB and SJV. For instance, overall normalized mean biases (NMBs) are 16% for SoCAB sites and -9% for SJV sites, and the respective Pearson correlation coefficients are 0.76 and 0.58. The relatively low correlation between predictions and observations for the SJV sites is due in part to poor performance at a site within the SJV domain but outside of the Valley. Due to the short simulation periods and the spatial and temporal sparseness of speciated $PM_{2.5}$ observations, only a limited model evaluation could be performed for PM. This evaluation suggests that the model did not adequately simulate the elevated $PM_{2.5}$ concentrations during the winter episodes. Simulating $PM_{2.5}$ episodes under cool, humid, and stagnant conditions in complex terrain remains an important area that requires focused research efforts (e.g., Baker et al., 2011; Hu et al., 2010). Since the current study is based on hypothetical scenarios, the reference case performance issues do not preclude a robust intercomparison of single-source modeling approaches; however, the $PM_{2.5}$ impacts discussed below may not be representative of the actual episodes simulated.

3.1 Impacts of NOx and VOC emissions on ozone

The impacts of NOx and VOC emissions on hourly average ozone estimated by B-F, (H)DDM, and APT are compared in Fig. 2 for surface cells in 84 × 84 km regions centered on the sources (see Fig. S16). Due to their common patterns, impacts are shown together in the panels for all emission levels, release heights, and source locations in an air basin. B-F and APT impacts are compared on a rank order basis because slight mismatches in space and time can occur due to the different model formulations. There is generally good agreement between (H)DDM and B-F impacts associated with the NOx and VOC sources in SoCAB (Fig. 2a), with slightly higher maximum impacts for HDDM than B-F in the NOx emissions cases. Differences in the HDDM and B-F impacts are due in part to the fundamental differences in the methods (e.g., the B-F impacts are first-order backward difference estimates of the first-order DDM sensitivities). Agreement between B-F and (H)DDM impacts for sources in SJV (Fig. 2b) is often better than for sources in SoCAB. A difference between SoCAB and SJV is the generally lower VOC-to-NOx ratios in SoCAB due to the large NOx emissions in LA and near the ports. For the B-F vs. APT comparisons (Fig. 2c and d), the central portions of the impact distributions agree closely, but APT tends to yield lower maximum impacts on ozone for NOx sources and higher maximum impacts for VOC sources. This behavior could occur if slightly more VOC-limited air masses mix with source emissions in the APT case than the standard B-F case; however, isolating the causes of the differences is difficult due to the complexity of the models and their different formulations.

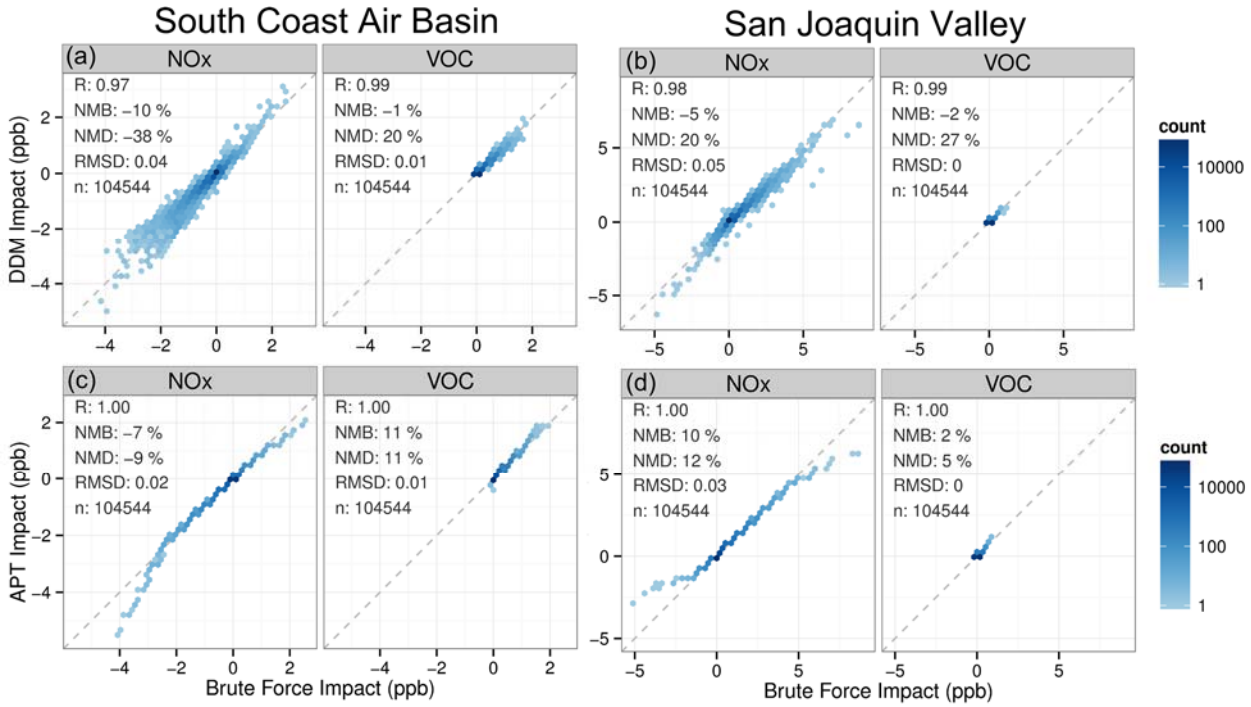

Fig. 2. Comparison of the impacts of NOx and VOC sources on hourly average O_3 (10-17 PST, 1-10 July 2007): (a) B-F vs. DDM in SoCAB, (b) B-F vs. DDM in SJV, (c) B-F vs. APT in SoCAB, and (d) B-F vs. APT in SJV. Impacts for B-F and APT are compared on a rank order basis. R: Pearson correlation coefficient; NMB: normalized mean bias; NMD: normalized mean difference; RMSD: root mean square difference; and n: number of samples. B-F is used as the reference case in statistics.

The impacts of the NOx sources in SoCAB on hourly average ozone are shown according to the corresponding VOC-to-NOx ratio in Fig. 3. At VOC-to-NOx ratios less than about 25 ppbC ppb^{-1}, the NOx sources frequently lead to a net decrease in ozone in all approaches due to the titration reaction and lower OH concentrations. The reverse pattern occurs for all approaches at higher VOC-to-NOx ratios, where increases in ozone are predicted with added NOx emissions. This behavior is consistent with our understanding of ozone chemistry and is evidence that the methods isolate SSIs and are not dominated by numerical noise.

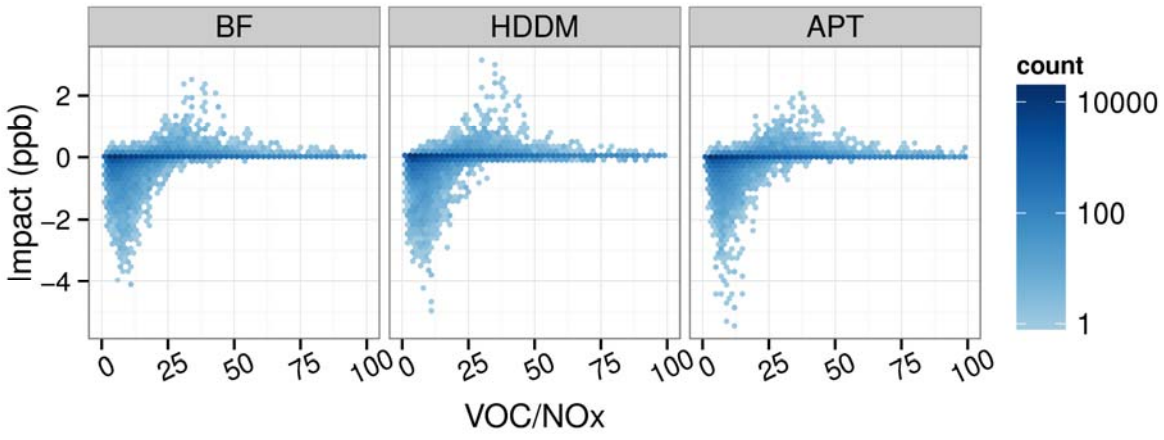

281

282 Fig. 3. Impacts of NOx sources in SoCAB on hourly average ozone (10-17 PST) as a function of VOC-
283 to-NOx ratio during 1-10 July 2007.

284 Examples of the spatial impacts of NOx emissions on maximum daily average 8-hr (MDA8)
285 O_3 are shown in Fig. 4 for an aloft source of NOx (100 t yr^{-1}) in Bakersfield during 7-9 July 2007.
286 Decreases in MDA8O_3 near the source and increases downwind are predicted by all three
287 methods with similar magnitudes and spatial patterns. The spatial patterns of impacts for this
288 source are driven by the orientation of the mountain ranges downwind of Bakersfield (Fig. 1).
289 The consistency in predictions among methods for this relatively small source builds confidence
290 that the approaches can identify SSIs for ozone.

291

292

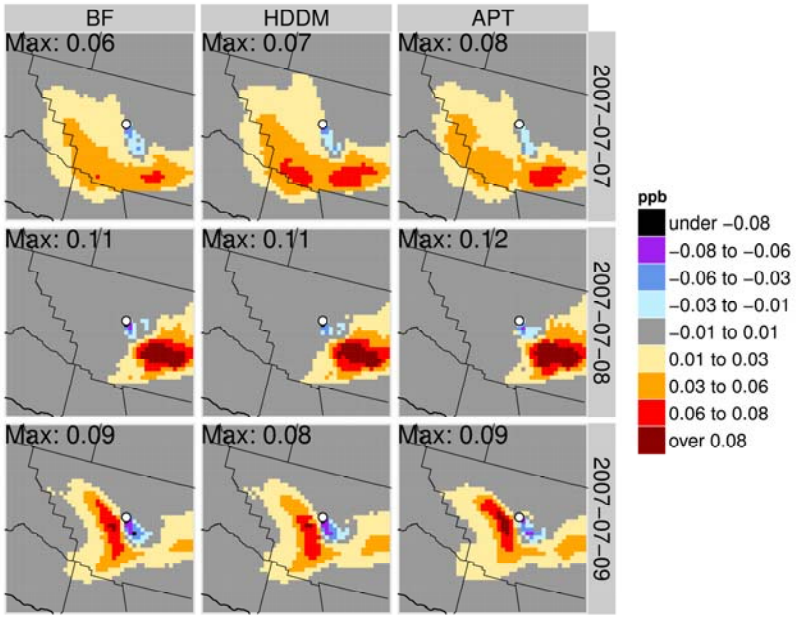

293

294 Fig. 4. Impacts of an aloft NOx source (100 t yr^{-1}) in Bakersfield on $MDA8O_3$ during 7-9 July 2007
295 estimated with the B-F, HDDM, and APT methods.

296 Although the different methods yield similar patterns of SSIs for the NOx source, the B-F
297 and HDDM approaches predict greater decreases in ozone near the source. For instance, the
298 maximum decrease is -0.1 ppb for B-F and HDDM and is -0.06 ppb for APT on 9 July for the case
299 in Fig. 4. More rapid mixing of NOx emissions to the surface in the Eulerian grid model
300 compared with the Lagrangian puff model used in APT has been reported previously and could
301 explain this difference. In Fig. 5, the difference in the average NOy impacts (APT - B-F) for a 500
302 t yr^{-1} release of NOx aloft in Pomona is shown. NOy is used here as a roughly conserved tracer
303 of the NOx emissions. For this release, APT predicts higher plume impacts than B-F aloft at the
304 source location (column 41), while B-F predicts higher plume impacts at the surface. The
305 greater mixing of NOx emissions to the surface in the source grid cell by B-F than APT can
306 explain the greater net ozone destruction there for aloft releases of NOx in the Eulerian grid
307 approaches (i.e., B-F and HDDM). The greater plume impacts aloft for APT persist downwind
308 until the plume reaches the surface near column 47 (Fig. 5) suggesting that APT would predict
309 maximum impacts slightly farther downwind than B-F or (H)DDM.

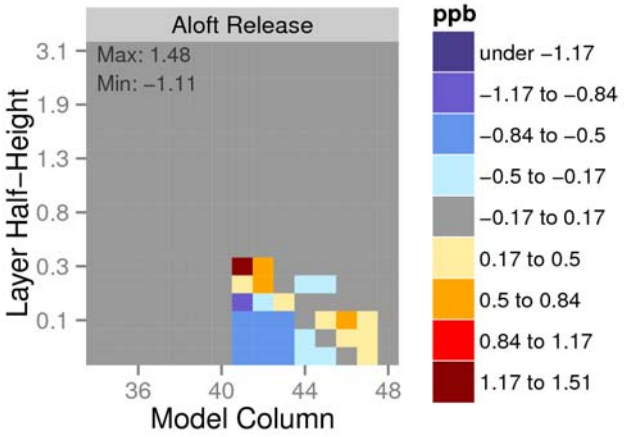

310

311 Fig. 5. Difference in average NOy impacts (APT – B-F) along the domain row containing the Pomona
312 NOx source (500 t yr^{-1} aloft) during 1-10 July 2007.

313 The maximum impacts of the NOx and VOC sources in SoCAB on $MDA8O_3$ during 1-9 July
314 2007 are shown in Fig. 6. Overall, there is consistency in the maximum impacts estimated by
315 the different methods. For the LA and Pomona sources, all methods indicate that VOC
316 emissions have greater maximum impacts on $MDA8O_3$ than NOx emissions. For the Riverside
317 source (located downwind of the LA urban area), NOx emissions have greater impacts than VOC
318 emissions on maximum $MDA8O_3$. The methods also yield a consistent pattern in terms of how
319 the maximum impacts vary across the emissions scenarios. Despite the general agreement,
320 however, the different methods lead to notable differences in maximum impacts on $MDA8O_3$ in
321 some NOx emissions cases: e.g., B-F yields higher maximum impacts than HDDM and APT for
322 the NOx sources in LA, and HDDM yields higher maximum impacts than B-F and APT for NOx
323 sources in Riverside. Maximum impacts on $MDA8O_3$ typically occur within about 25 km of the
324 source for all methods (e.g., Fig. 7), with APT peaks being slightly farther downwind than the B-
325 F and (H)DDM peaks as discussed above. Comparisons of maximum impacts on $MDA8O_3$
326 estimated for the SJV sources demonstrate a similar level of agreement as for the SoCAB
327 sources (Fig. S17 and S18).

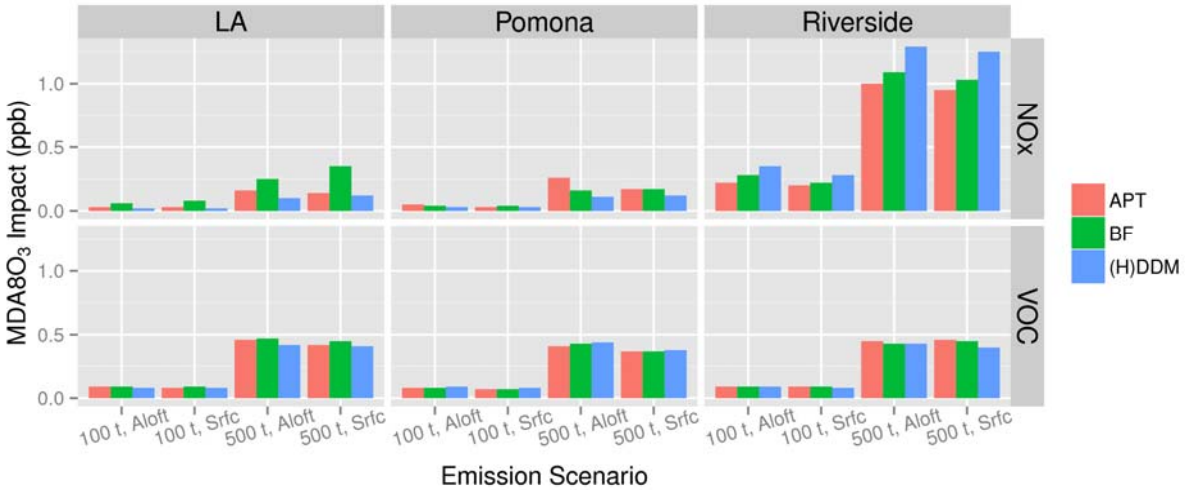

328

329 Fig. 6. Maximum impacts of NOx and VOC emission sources in SoCAB on $MDA8O_3$ during 1-9 July
330 estimated by the B-F, (H)DDM, and APT methods.

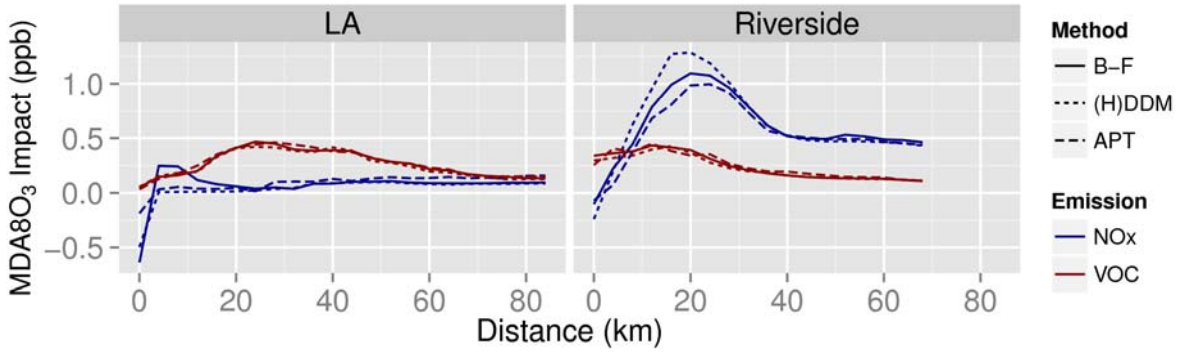

331

332 Fig. 7. Maximum impacts of NOx and VOC emissions (500 t yr^{-1} aloft) on $MDA8O_3$ during 1-9 July as a
333 function of distance from the LA and Riverside sources as estimated by the B-F, (H)DDM, and APT
334 methods.

335 Finally, good agreement was found among methods for the relative change in ozone
336 impacts for the near-surface releases compared with the aloft releases and for the 500 t yr^{-1}
337 emission cases compared with the 100 t yr^{-1} cases. The slopes of the best-fit lines for near-
338 surface vs. aloft release impacts on hourly average ozone are provided in Table 3 and Fig. S20.
339 These values are similar among methods and suggest that the maximum difference in ozone
340 impacts would be about 20% for the VOC sources and 10% for the NOx sources when emissions
341 are released near the surface compared with aloft. This weak sensitivity of ozone impacts to

release height helps explain why the differences in initial plume transport for the APT and Eulerian approaches discussed above do not necessarily lead to large differences in maximum impacts for ozone. The slopes of the best-fit lines for hourly average ozone impacts from the 500 vs. 100 t yr^{-1} sources are provided in Table 4 and Fig. S21. These values agree to within 10% for the different methods and indicate that increasing emissions from 100 to 500 t yr^{-1} would increase ozone impacts by factors of 4.1 to 5 depending on the conditions.

Table 3. Slope of the least-squares fit line for aloft vs. near-surface release impacts on hourly average ozone[a,b]

	B-F		(H)DDM		APT	
	NOx	VOC	NOx	VOC	NOx	VOC
SoCAB	0.99	0.89	1.1	0.9	0.93	0.91
SJV	1	1.2	1	1.2	0.96	1.2

[a]e.g., a value of 1.1 indicates 10% greater impacts for near-surface than aloft releases during 1-10 July (10-17 PST).
[b]See Fig. S20 for details on best-fit line

Table 4. Slope of the least-squares fit line for 100 vs. 500 t yr^{-1} emissions impacts on hourly average ozone[a,b]

	B-F		(H)DDM		APT	
	NOx	VOC	NOx	VOC	NOx	VOC
SoCAB	4.8	4.9	4.8	5	4.9	5
SJV	4.1	4.9	4.1	4.8	4.5	5

[a]e.g., a value of 5 indicates a factor of 5 greater impacts for 500 than 100 t yr^{-1} emissions rates.
[b]See Fig. S21 for details on best-fit line

3.2 $PM_{2.5}$ impacts

The impacts of primary $PM_{2.5}$ emissions from the SoCAB and SJV sources on primary $PM_{2.5}$ concentrations were compared for the B-F, DDM, and APT approaches. Impacts estimated with the B-F and DDM approaches were nearly identical indicating that primary pollutant concentrations respond linearly to the emissions (Fig. S22). Some disagreement is evident in primary $PM_{2.5}$ impacts calculated from the APT approach compared with impacts from the B-F and DDM approaches, particularly during evening and night hours (Fig. S23 and S24). These differences suggest that primary pollutant impacts are sensitive to the differences in mixing discussed above for the Eulerian grid and Lagrangian puff models, especially when

mixing heights are low. Similarly, the primary $PM_{2.5}$ impacts for near-surface releases were more than six times those for aloft releases in SoCAB (Fig. S25) in contrast with the relative insensitivity to release height for ozone impacts.

The impacts of SO_2 sources in SJV on hourly average $PM_{2.5}$ sulfate concentrations agree well among all methods for the July period (Fig. 8). The methods also yielded similar spatial patterns of impacts on 24-hr average $PM_{2.5}$ sulfate. For instance, the impacts of the aloft Shafter source (100 t yr^{-1}) on 8 July are directed southward down the Valley for all methods (Fig. 9). In this case, all methods had the same domain-wide maximum impact despite a tendency for APT to have smaller impacts near the source than B-F and DDM. For the January period, impacts of the SO_2 sources in SJV on sulfate also agreed well for the B-F and DDM approaches, but the APT impacts were slightly lower at the high end of the impacts distribution (Fig. S26).

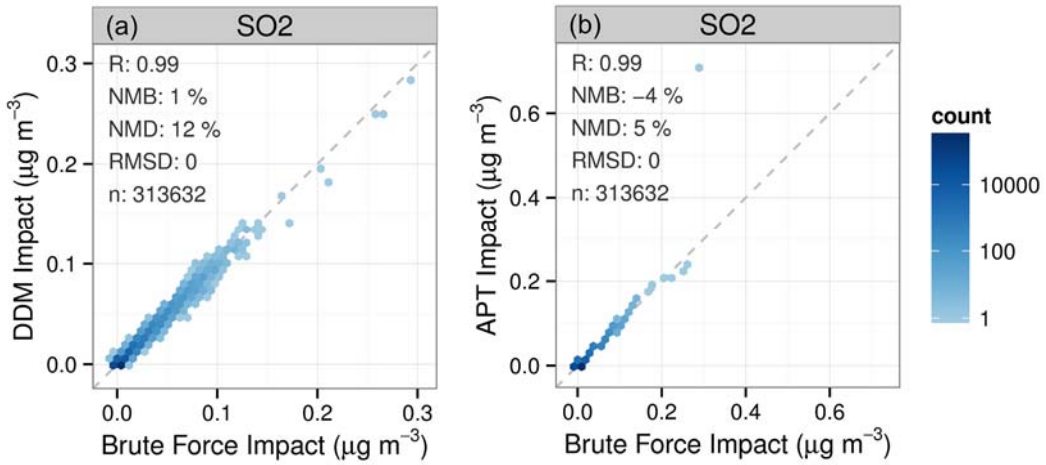

Fig. 8. Comparison of the impacts of SO_2 sources in SJV during 1-10 July 2007 on hourly average $PM_{2.5}$ sulfate: (a) B-F vs. DDM and (b) B-F vs. APT. Impacts for B-F and APT are compared on a rank order basis.

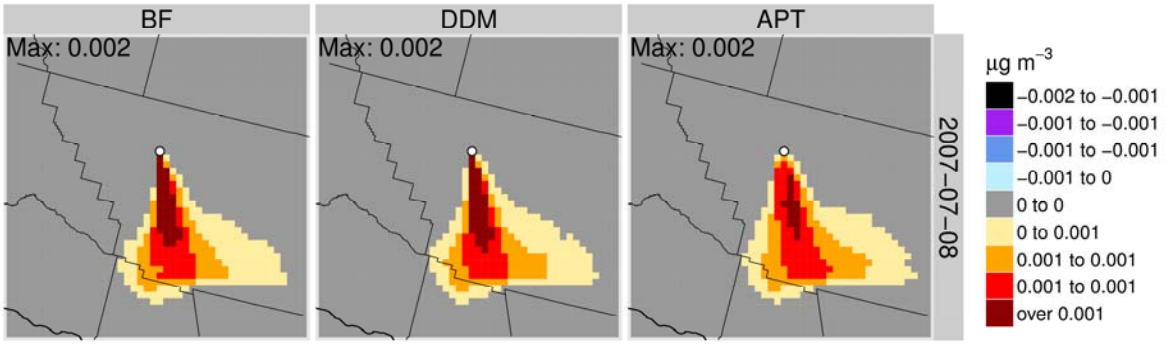

383

384 Fig. 9. Impacts of an aloft SO_2 source (100 t yr^{-1}) in Shafter on 24-hr average $PM_{2.5}$ sulfate on 8 July
385 2007 estimated by B-F, HDDM, and APT methods.

386 The maximum impacts of SO_2 sources in SJV on 24-hr average $PM_{2.5}$ sulfate during the July
387 period are shown in Fig. 10. There is generally good agreement in maximum impacts among
388 the methods with the highest values ranging from 0.06 µg m^{-3} (APT and DDM) to 0.07 µg m^{-3} (B-
389 F) for the 500 t yr^{-1} near-surface release in S. Bakersfield. Similar to the findings for ozone, the
390 maximum impacts of the SO_2 sources on 24-hr average sulfate typically occur within about 25
391 km of the source in all methods (e.g., Fig. S27).

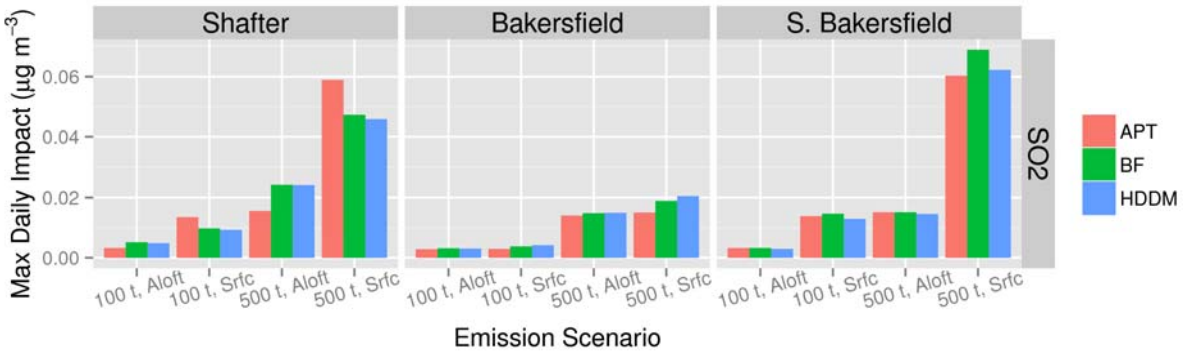

392

393 Fig. 10. Maximum impacts of SO_2 emission sources in SJV on 24-hr average $PM_{2.5}$ sulfate
394 concentrations during 1-9 July 2007 estimated by the B-F, DDM, and APT methods.

395 There is greater disagreement among methods for NOx and NH_3 source impacts on
396 $PM_{2.5}$ nitrate than for SO_2 source impacts on $PM_{2.5}$ sulfate. For NOx emissions sources, the
397 Pearson correlation between hourly average nitrate impacts for the HDDM and B-F approaches

is less than 0.1 in all cases (e.g., Fig. S28). The poor correlation is due to numerical instabilities in the DDM sensitivity calculations for our simulation conditions, and model development is ongoing to resolve them. Agreement is better between the APT and B-F estimates of NOx and NH_3 source impacts on hourly average nitrate than between the (H)DDM and B-F estimates. For instance, the Spearman correlation between the APT and B-F impact estimates is 0.99 for NH_3 sources and 0.8 for NOx sources in SoCAB during the November period (Fig. 11). In the SoCAB simulations, the impacts of NH_3 sources on nitrate are generally greater than the impacts of NOx sources on nitrate. Previous studies have found that nitrate formation in eastern SoCAB is more limited by the availability of NH_3 than HNO_3 and that NH_3 emissions from dairy facilities near Chino may be underestimated in the model (Nowak et al., 2012; Kelly et al., 2014). These characteristics are conducive to a large responsiveness of nitrate concentrations to NH_3 emission changes. The NH_3 sources could also lead to relatively high nitrate impacts because ammonium nitrate can form instantly in response to NH_3 emissions, whereas NOx emissions must first react to form HNO_3 and become diluted in the meantime.

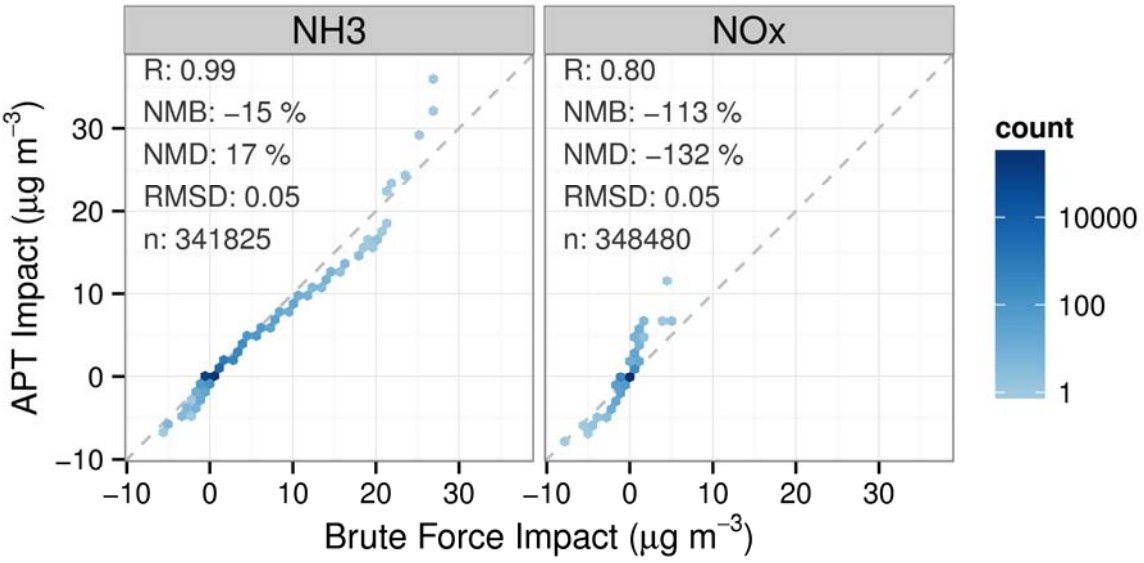

Fig. 11. Comparison of the impacts of NH_3 and NOx sources in SoCAB on hourly average $PM_{2.5}$ nitrate during 2-12 November for the B-F and APT approaches. Impacts are compared on a rank order basis.

Despite the good correlation in the B-F and APT nitrate impacts for NOx and NH_3 sources in SoCAB, there can be substantial bias in the impacts for the NOx sources (Fig. 11). A similar level of disagreement is also evident in the B-F and APT nitrate impacts for the SJV sources, with APT yielding a wider range of impacts than B-F (Fig. S29). Comparisons of the spatial patterns of nitrate impacts suggest that the differences between B-F and APT estimates could be related to numerical artifacts associated with brute-force differencing. In Fig. 12, spatial fields of the impacts of a 100 t yr^{-1} aloft source of NOx in Pomona on 24-hr average nitrate are shown for the B-F and APT approaches on 9 and 10 November, which were selected as representative days. The B-F method predicts reductions in nitrate in a plume to the east of the source on 9 November in response to the NOx emissions, whereas APT predicts increases in nitrate close to the source. The inverse relationship between nitrate concentration changes and NOx emissions changes predicted by the B-F method for this plume has been identified previously in studies of oxidant limited areas (e.g., Pun and Seigneur, 2001). Away from the source, the APT approach yields a checkered pattern of positive and negative impacts that are often larger in magnitude than the values in the plume near the source (Fig. 12, upper right). The grid cells with relatively large nitrate impacts do not correspond to locations with large NH_3 emissions in the model that could explain the distinct increases in nitrate. The checkered pattern of nitrate impacts away from the source for the APT approach combined with a previous finding that nitrate predictions of the inorganic aerosol module are susceptible to numerical instabilities (Bhave et al., 2011) suggest that numerical errors may affect the nitrate impact estimates in this case. The apparently smaller influence of numerical errors on the B-F than APT estimates may be related to the more complex algorithms of the CMAQ-APT model, which simulates and merges nonlinearly evolving processes in Lagrangian and Eulerian frameworks, than the standard CMAQ model.

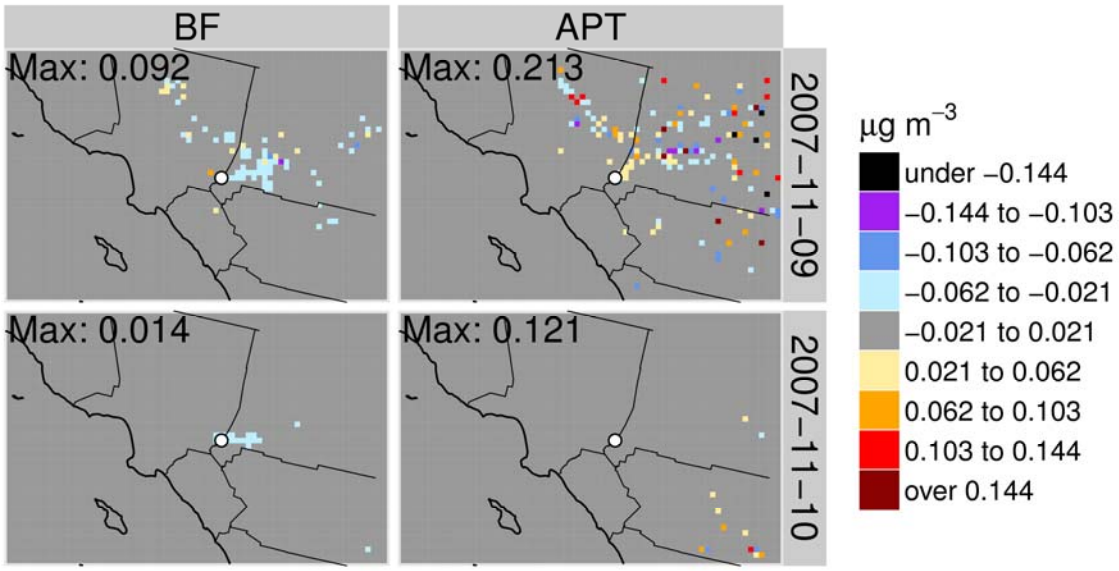

Fig. 12. Impacts of an aloft NOx source (100 t yr^{-1}) in Pomona on 24-hr average $PM_{2.5}$ nitrate on 8-9 November estimated by the B-F and APT methods.

4. Conclusions

The B-F, (H)DDM, and APT methods for estimating SSIs for $PM_{2.5}$ and ozone were compared under a wide range of conditions (i.e., emissions amount and composition, source location, and stack parameters). There is consistency in the impacts of NOx and VOC sources on ozone and SO_2 sources on $PM_{2.5}$ sulfate calculated by these methods. This consistency is evident in the similar magnitudes, spatial patterns, and strong correlations among the impacts. Also, the impact estimates vary similarly for the methods with variations in the VOC-to-NOx ratio and the source release height. The agreement in results for the (H)DDM and brute-force differencing methods indicates that numerical noise associated with differencing did not obscure the source impacts estimated with B-F and APT for these species. It also demonstrates that extrapolation of (H)DDM sensitivities from the full emissions level to the zero-out level yields similar results as differencing simulated fields for the full emissions level and zero-out level. Disagreement among methods is evident in the $PM_{2.5}$ nitrate impacts associated with NH_3 and NOx sources. Numerical instabilities in (H)DDM sensitivity calculations compromise the nitrate impact estimates from that approach. The B-F and APT methods, which use brute-force differencing to

459 estimate nitrate impacts, are affected by numerical artifacts to a lesser degree than (H)DDM,
460 with the artifacts being more prominent for APT than B-F. The influence of numerical noise on
461 the APT-based nitrate impacts is greater in magnitude than the maximum source impacts in
462 some cases. Overall, our results indicate that the (H)DDM, B-F, and APT approaches are viable
463 for use in estimating SSIs for ozone and secondary $PM_{2.5}$ sulfate, while the B-F method appears
464 to be most reliable for estimating nitrate impacts. Additional field study measurements of
465 source impacts are needed to supplement previous model evaluations and better constrain
466 model estimates of SSIs.

467

468 **5. Acknowledgements**

469 The authors thank Prakash Karamchandani for helpful discussions on CMAQ-APT. We
470 acknowledge Alan Beidler, Kathy Brehme, Chris Misenis, and Lara Reynolds for developing
471 CMAQ model inputs. We also thank Rohit Mathur and Norm Possiel for providing helpful
472 comments on the draft manuscript. **Disclaimer**: Although this work was reviewed by EPA and
473 approved for publication, it may not necessarily reflect official Agency policy.

474

6. References

Baker, K. R., Misenis, C., Obland, M.D., Ferrare, R. A., Scarino, A., Kelly, J.T., 2013. Evaluation of surface and upper air fine scale WRF meteorological modeling of the May and June 2010 CalNex period in California, Atmos. Environ., 8, 299–309.

Baker, K.R., Hawkins, A., Kelly, J.T., 2014. Photochemical grid model performance with varying horizontal grid resolution and sub-grid plume treatment for the Martins Creek near-field SO2 study. Atmos. Environ., 99, 148-158.

Baker, K. R., Kelly, J. T., 2014. Single source impacts estimated with photochemical model source sensitivity and apportionment approaches, Atmos. Environ., 96, 266-274.

Baker, K.R., Simon, H., Kelly, J.T., 2011. Challenges to modeling "cold pool" meteorology associated with high pollution episodes. Environ. Sci. Technol., 45, 7118–7119.

Bhave, P.V., Sarwar, G., Pye, H.O.T., Pouliot, G., Simon, H., Young, J., Nolte, C.G., Schere, K., Mathur, R., 2011. Impact of ISORROPIA II on air quality model predictions. Commmunity Modeling and Analysis System Conference, Chapel Hill, NC October 24-26, 2011. Available from https://www.cmascenter.org/conference/2011/agenda.cfm

Byun, D., Schere, K.L., 2006. Review of the governing equations, computational algorithms, and other components of the models-3 Community Multiscale Air Quality (CMAQ) modeling system. Appl. Mech. Rev. 59, 51-77.

Cimorelli, A. J., Perry, S.G., Venkatram, A., Weil, J.C., Paine, R.J., Wilson, R.B., Lee, R.F., Peters, W.D. Brode, R.W., 2005. AERMOD: A Dispersion Model for Industrial Source Applications. Part I: General Model Formulation and Boundary Layer Characterization. J. Appl. Meteor., 44, 682–693. doi: http://dx.doi.org/10.1175/JAM2227.1

Cohan, D.S., Hakami, A., Hu, Y., Russell, A.G., 2005. Nonlinear response of ozone to emissions: Source apportionment and sensitivity analysis. Environ. Sci. & Technol., 39, 6739-6748.

ENVIRON, 2014. User's Guide Comprehensive Air Quality Model with Extensions. ENVIRON International Corporation, Novato. www.camx.com.

Gillani, N. V., Pleim, J. E., 1996. Subgrid scale features of anthropogenic emissions of NOx and VOC in the context of regional Eulerian models. Atmos. Environ., 30, 2043–2059.

Hakami A., Odman, M.T., Russell, A.G., 2003. High-order, direct sensitivity analysis of multidimensional air quality models. Environ. Sci. Technol., 37 (11), 2442-2452.

Hakami A., Odman, M.T., Russell, A.G., 2004. Nonlinearity in atmospheric response: A direct sensitivity analysis approach. J. Geophys. Res.-Atmos., 109 (D15), Art. No. D15303.

Henderson, B.H., Jeffries, H.E., Kim, B.-U., Vizuete, W.G., 2010. The influence of model resolution on ozone in industrial volatile organic compound plumes. J. Air Waste Manag. Assoc., 60 (9), 1105-1117, DOI: 10.3155/1047-3289.60.9.1105.

Henderson, B.H., Kimura, Y., McDonald-Buller, E., Allen, D.T., Vizuete, W., 2011. Comparison of Lagrangian process analysis tools for Eulerian air quality models. Atmos. Environ., 45(29), 5200-5211.

Hu, J., Ying, Q., Chen, J., Mahmud, A., Zhao, Z., Chen, S.-H., Kleeman, M.J., 2010. Particulate air quality model predictions using prognostic vs. diagnostic meteorology in central California. Atmospheric Environment, 44 (2), 215–226.

Karamchandani, P., Johnson, J., Yarwood, G., Knipping E, 2014. Implementation and application of sub-grid-scale plume treatment in the latest version of EPA's third-generation air quality model, CMAQ 5.01. J. Air Waste Manag. Assoc. 64 (4), 453-67.

Karamchandani, P., Seigneur, C., Vijayaraghavan, K., Wu, S., 2002. Development and application of a state-of-the-science plume-in-grid model. J. Geophys. Res., 107 (D19), 4403, doi:10.1029/2002JD002123

Karamchandani, P., Vijayaraghavan, K., Chen, S.-Y., Seigneur, C., Edgerton, E.S., 2006. Plume-in-grid modeling for particulate matter. Atmos. Environ., 40, 7280–7297.

Karamchandani, P., Vijayaraghavan, K., Yarwood, G., 2011. Sub-grid scale plume modeling. Atmosphere 2 (3), 389-406.

Kelly, J.T., Baker, K.R., Nowak, J.B., Murphy, J.G., Markovic, M.Z., VandenBoer, T.C, Ellis, R.A., Neuman, J.A., Weber, R.J., Roberts, J.M., Veres, P.R., de Gouw, J.A., Beaver, M.R., Newman, S., Misenis, C., 2014. Fine-scale simulation of ammonium and nitrate over the South Coast Air Basin and San Joaquin Valley of California during CalNex-2010, J. Geophys. Res. Atmos., 119, doi:10.1002/2013JD021290.

Kim, Y., Seigneur, C., Duclaux, O., 2014. Development of a plume-in-grid model for industrial point and volume sources: application to power plant and refinery sources in the Paris region, Geosci. Model Dev., 7, 569-585, doi:10.5194/gmd-7-569-2014.

Korsakissok, I. and Mallet, V., 2010. Development and application of a reactive plume-in-grid model: evaluation over Greater Paris. Atmos. Chem. Phys., 10, 8917-8931.

Mathur, R., Peters, L.K., Saylor, R.D., 1992. Sub-grid representation of emission source clusters in regional air quality modeling, Atmos. Environ., 26A(17), 3219-3238.

Napelenok, S.L., Cohan, D.S., Odman, M.T., Tonse, S., 2008. Extension and evaluation of sensitivity analysis capabilities in a photochemical model. Environmental Modelling & Software, 23 (8), 994–999.

Nowak, J. B., Neuman, J.A., Bahreini, R., Middlebrook, A.M., Holloway, J.S., McKeen, S.A., Parrish, D.D., Ryerson, T.B., Trainer, M., 2012. Ammonia sources in the California South Coast Air Basin and their impact on ammonium nitrate formation. Geophys. Res. Lett., 39, L07804, doi:10.1029/2012GL051197.

Pun, B.K., Seigneur, C., 2001. Sensitivity of particulate matter nitrate formation to precursor emissions in the California San Joaquin Valley. Environ. Sci. Technol., 35(14), 2979-2987.

Pusede, S. E., Cohen, R.C., 2012. On the observed response of ozone to NOx and VOC reactivity reductions in San Joaquin Valley California 1995-present. Atmos. Chem. Phys., 12(18), 8323–8339, doi:10.5194/acp-12-8323-2012.

Ryerson, T. B., Andrews, A.E., Angevine, W.M., Bates, T.S., Brock, C.A., Cairns, B., Cohen, R.C., Cooper, O.R., de Gouw, J.A., Fehsenfeld, F.C., Ferrare, R.A., Fischer, M.L., Flagan, R.C., Goldstein, A.H., Hair, J.W., Hardesty, R.M., Hostetler, C.A., Jimenez,J.L., Langford, A.O., McCauley, E., McKeen, S.A., Molina, L.T., Nenes, A., Oltmans, S.J., Parrish, D.D., Pederson, J.R., Pierce, R.B., Prather, K., Quinn, P.K., Seinfeld, J.H., Senff, C.J., Sorooshian, A., Stutz, J., Surratt, J.D., Trainer, M., Volkamer, R., Williams, E.J., Wofsy, S.C., 2013. The 2010 California Research at The Nexus of Air Quality and Climate Change (CalNex) field study, J. Geophys. Res. Atmos., 118, 5830–5866, doi:10.1002/jgrd.50331.

552 Skamarock, W. C., Klemp, J.B., Dudhia, J., Gill, D.O., Barker, D.M., Duda, M., Huang, X.-Y., Wang, W.,
553 Powers, J.G., 2008. A description of the Advanced Research WRF Version 3. NCAR Technical Note,
554 NCAR/TN–475+STR.

555 Seigneur, C., Tesche, T., Roth, P., Liu, M., 1983. On the treatment of point source emissions in urban air
556 quality modeling. Atmos. Environ., 17, 1655–1676.

557 U.S. Environmental Protection Agency, 2012a. "Sierra Club Petition Grant". Gina McCarthy
558 Administrative Action dated January 4, 2012. U.S. Environmental Protection Agency, Washington,
559 District of Columbia 20460.
560 http://www.epa.gov/ttn/scram/10thmodconf/review_material/Sierra_Club_Petition_OAR-11-002-
561 1093.pdf

562 U.S. Environmental Protection Agency, 2012b. Preparation of Emissions Inventories for the Version 5.0,
563 2007 Emissions Modeling Platform.
564 http://epa.gov/ttn/chief/emch/2007v5/2007v5_2020base_EmisMod_TSD_13dec2012.pdf.

565 U.S. Environmental Protection Agency, 2013a. Air Quality Modeling Technical Support Document for the
566 2007 Fine Scale Modeling Platform, November.
567 http://www.epa.gov/ttn/scram/reports/FineScalePlatform2007_ModelingTSD.pdf

568 U.S. Environmental Protection Agency, 2013b. Meteorological Model Performance, 2007 Fine Scale
569 Platform, November. http://www.epa.gov/ttn/scram/reports/WRF_2007_FineScale_Performance.pdf

570 U.S. Environmental Protection Agency, 2014. Guidance for PM2.5 Permit Modeling.

571 EPA-454/B-14e001.
572 http://www.epa.gov/scram001/guidance/guide/Guidance_for_PM25_Permit_Modeling.pdf

573 Whitten, G.Z., Heo, G., Kimura, Y., McDonald-Buller, E., Allen, D.T., Carter, W.P.L., Yarwood, G., 2010. A
574 new condensed toluene mechanism for Carbon Bond CB05-TU. Atmospheric Environment 44, 5346-
575 5355

576 Yang, Y.J., Wilkinson, J., Russell, A.G., 1997. Fast, direct sensitivity analysis of multidimensional
577 photochemical models. Environ. Sci. Technol., 31, 2859-2868.

578 Yarwood, G., Rao, S., Yocke, M.,Whitten, G.Z., 2005. Updates to the Carbon Bond Mechanism: CB05. US
579 EPA Final Report, 161 pp. Available at http://www.camx.com/publ/pdfs/CB05_Final_Report_120805.pdf

580 Zhang, W., Capps, S.L., Hu, Y., Nenes, A., Napelenok, S.L., Russell, A.G., 2012. Development of the high-
581 order decoupled direct method in three dimensions for particulate matter: enabling advanced sensitivity
582 analysis in air quality models. Geosci. Model Dev., 5, 355-368.

583 Zhou, W., Cohan, D.S., Pinder, R.W., Neuman, J.A., Holloway, J.S., Peischl, J., Ryerson, T.B., Nowak, J.B.,
584 Flocke, F., Zheng, W.G., 2012. Observation and modeling of the evolution of Texas power plant plumes.
585 Atmos. Chem. Phys., 12, 455-468.